Bulletin of the JSME Vol.19, No.3, 2024
Journal of Fluid Science and Technology

A study of the spatiotemporal structure of a turbulent boundary layer measured by the use of two hot-wire probes (Velocity time series patterns and Kolmogorov's structure function)

Masashi ICHIMIYA* and Ikuo NAKAMURA**
* Department of Mechanical Science, Tokushima University
2-1 Minami-Josanjima-cho, Tokushima-shi, Tokushima 770-8506, Japan
E-mail: ichimiya@tokushima-u.ac.jp
** Emeritus Professor, Nagoya University
Furo-cho, Chikusa-ku, Nagoya-shi, Aichi 464-8601, Japan

Received: 5 November 2023; Revised: 12 February 2024; Accepted: 22 April 2024

Abstract
The streamwise velocity at two points in a turbulent boundary layer under zero pressure gradient was measured using two hot-wire probes separated in the wall-normal direction. The time trace of the fluctuating velocity difference, probability density function, fluctuating vorticity, structure function, and the spatial correlation coefficient was obtained. First, the physical importance of structure functions was explained in some detail. Then, the results of the measurements were considered. When the spatial separation between two points is small, the fluctuating velocity difference decreases monotonically as the two points move away from the wall. On the other hand, as the spatial separation increases, the similarity between the two fluctuating velocities decreases. In addition, the fluctuating velocity at the nearer point from the wall becomes dominant. When moving away from the wall, the fluctuating velocity difference first increases, then reaches a maximum, and finally decreases. When both positions are within the logarithmic region or defect region, the velocity difference is made between similar fluctuating velocities. Hence, the probability density function distribution shape is symmetrical with respect to positive and negative values, close to the Gaussian distribution. The fluctuating vorticity decreases monotonically as it moves away from the wall, regardless of the spatial separation. The structure function increases as the separation increases. Away from the wall, the length over which the correlation is maintained increases, resulting in a large eddy.

Keywords : Boundary layer, Turbulence, Structure function, Spatial correlation, Spatiotemporal structure, Two-point velocity difference

1. Introduction

1.1 The physical significance of the spatiotemporal structure of a turbulent boundary layer

Until now, in mechanical engineering, the main problem of the turbulent boundary layer has been the distribution of wall shear stress in the streamwise direction. For a typical example of a flow field around a cylinder in a uniform stream, researchers' interest is concentrated on the problem of wall shear stress profile along the cylinder arc length, since it determines the boundary layer separation point and that is the crucial factor of pressure drag of the cylinder, see Schlichting and Gersten (2000). In a real fluid mechanical engineering problem, the scenario is similar to that of a pump and a blower, where the mean velocity distribution and turbulence intensity profile are critical for determining skin friction.

On the other hand, boundary layer problems are important not only for mechanical and aeronautical engineering but also for very tall building architecture, large suspension bridges, and environmental problems. In such problems, we must have not only the knowledge of skin friction but also the spatiotemporal varying structure of wind, which has widespread scales from the Kolmogorov dissipation scale to the Tayler integral scale. These problems are described in detail in the large book "Structure Endure Engineering to Wind (1997)". The recent development of large-scale wind turbines has

Paper No.23-00502
[DOI: 10.1299/jfst.2024jfst0028]

created a demand to improve the efficiency of wind farms (Goit and Meyers, 2014). Then, it is important to analyze the atmospheric boundary layer's spatiotemporal structure for the design of wind turbines.

In the present-day world, wind farms are constructed as a solution to decreasing carbon dioxide concentration in the atmosphere to prevent global warming. In such a problem we must know the horizontal turbulent structure of the atmospheric boundary layer, which is discussed in great detail in Garratt (1992) and Wyngaard (2010).

1.2 The spatiotemporal structure description of the turbulent boundary layer

In this study, we performed experiments about a flat plate turbulent boundary layer using two hot-wire anemometers, as shown in Fig.1. This boundary layer is so fundamental. It is very important to understand its spatiotemporal structure not only on the physical side but also in various fields such as aeronautical, mechanical, architectural, and environmental engineering. For the sake of obtaining such a complicated structure, it is important to have an insight into the pattern of the hot-wire output time series signal which indicates glimmered turbulent velocity. As a result, in the following, we will present the time series records of hot-wire signals and explain their behaviors. Then, graphs of the structure function of turbulence in the boundary layer, which was introduced by Kolmogorov (1941), will be shown.

Kolmogorov's paper, published in 1941, is very frequently cited among turbulence researchers. It is cited in abbreviated, very compact form as K41 and has the name of a seminal paper. His structure function is very intricate quantity, so we try to explain its physical significance somewhat in detail. Within our survey, we have not found any paper that explains the physical meanings of the structure function.

The spatial structure of turbulent flow was first analyzed in Taylor's series of papers (Taylor, 1935), which introduced the correlation of the two spatial points. Von Kármán and Howarth (1938) obtained its equation, which has the name Kármán-Howarth equation, but the equation is not closed. Then, the notorious closure problem appeared because of the nonlinearity of Navier-Stokes equations.

In K41, a very new and strange quantity was introduced to discuss the spatiotemporal structure of turbulence, that is, to set two spatial points, A and B, as shown in two hot-wire probes used in our experiment (Fig. 1(a)), and two different times t and $t(0)$ at these two spatial points. Then, the instantaneous velocity difference was considered. They have two components, one of which is directed from A to B, and the other is orthogonal to it. In Kolmogorov's field, a point has coordinated components as (x_1, x_2, x_3, t), i.e., four-dimensional space is set. Note that the usual velocity measuring time is the same for every space point, but if the space point in K41 is different, then each velocity measuring time may differ. This physical quantity has no name in K41, but the following papers used the name of structure function, see Anselmet et al. (1984), Hill (2001), and Gatti et al. (2020) for this term. However, some authors use the name of velocity difference or velocity increment.

K41 proposes the constraint of local homogeneity and local isotropy condition on the structure function, then the first and second similarity assumptions are set down. After that, in the case of a very large Reynolds number, K41 considers the probability distribution of the structure function expressed as,

$$w_\alpha(P) = u_\alpha(P) - u_\alpha(P(0)),\ \alpha = 1, 2, 3, \tag{1}$$

where α means coordinate directions as usual. P and $P(0)$ are defined as $P = (x_1, x_2, x_3, t)$, $P(0) = (x_1(0), x_2(0), x_3(0), t(0))$, so the structure function in K41 has special meaning. Moreover, velocity measuring time is different between two spatial points. Then the study is carried out using a coordinate system of (x_1, x_2, x_3, t) in four dimensions.

Kolmogorov did not use any figures or graphs. We employ Fig. 2, which we created, to provide an understandable explanation of the structure function's physical importance. Set a material point A as indicated in the figure. The A is a point in an eddy, which means a material lump of turbulent fluid, and we define an orthogonal coordinate (x_1, x_2, x_3) which has the origin at A as shown. The u_A is the velocity vector measured at A at the time t. It has x_i-component as u_{Ai}. The second point, B, is set as shown in Fig. 2. The position vector $\boldsymbol{r}$ of B relative to A is that,

$$\boldsymbol{r} = (r_1, r_2, r_3), \tag{2}$$

and then the velocity vector at B at time $t + \tau$ is written as $\boldsymbol{u_B}$, i.e.,

[DOI: 10.1299/jfst.2024jfst0028]

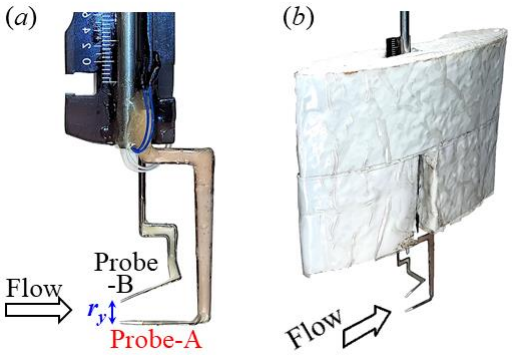

Fig. 1 Photographs of two hot-wire probes with a caliper for separation adjustment are (*a*) visible and (*b*) wrapped in a streamlined cover.

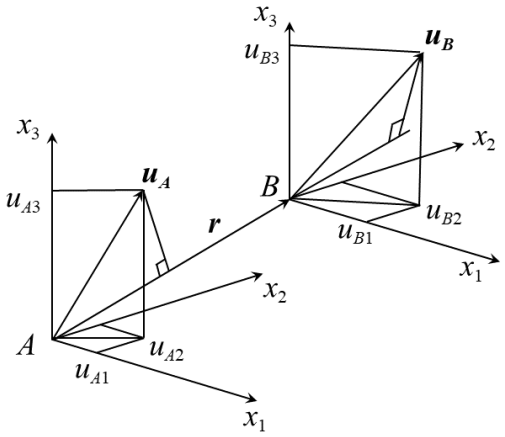

Fig. 2 Schematic of two-point velocity.

$$\boldsymbol{u_A} = \boldsymbol{u}(\boldsymbol{x}, t) = \boldsymbol{u}(x_1, x_2, x_3, t), \tag{3-1}$$

$$\boldsymbol{u_B} = \boldsymbol{u}(\boldsymbol{x} + \boldsymbol{r}, t + \tau) = \boldsymbol{u}(x_1 + r_1, x_2 + r_2, x_3 + r_3, t + \tau). \tag{3-2}$$

In K41, the coordinate (x_1, x_2, x_3, t) is defined as above, and then a very new coordinate y_α is introduced as follows,

$$y_\alpha = x_\alpha - x_\alpha^{(0)} - u_\alpha(P^{(0)})(t - t^{(0)}),\ s = t - t^{(0)}. \tag{4}$$

Since coordinate y_α of point P depends on the random variable $u_\alpha(P^{(0)})$ as shown in Eq. (4), then the coordinate y_α is also a random variable. This attention is paid to K41, but standard textbooks of turbulence written by Hinze (1975a), Pope (2000), and Davidson (2015a) do not use this random coordinate system. Moreover, in K41, the reason why this coordinate is used is not explained.

As noted above, in K41, the velocity vector at points A and B is measured at time t and $t + \tau$, respectively, Then, it is resolved in the r-component, which has the direction from point A to point B, and it has another component perpendicular to it. Finally, the difference between these components is discussed; namely, K41 introduced very new physical quantities.

Let us consider the physical meaning of this velocity difference in the case of a flat plate turbulent boundary layer, as shown in Fig. 3. Where Z is a name that indicates a material lump that includes material point A and moves following the flow field between time t and $t + \Delta t$ as shown in Fig. 3. The eddy name Z is invariant since it indicates the lump of fluid which moves. Z has a Lagrangian coordinate nature of the flow. Then the lump of eddy Z moves, and material point A in Z also moves to A' after Δt. In K41, the time difference, s appeared in Eq. (4), is not necessarily small, but in Fig. 3, the time difference Δt is taken to be small for the sake of the meaning of the figure to be clear physically. Then, the velocity difference used in K41 is evident from the figure that the idea comes from Prandtl's mixing length model (Prandtl, 1925), which is also based on the concept of fluid material lump Z's movement during time Δt conserving its momentum. In the mixing length model, Z moves along the mixing length l with constant momentum After the motion, it mixes with the surrounding new fluid instantaneously. Then, it produces a change in the momentum of the Eulerian field. In K41, Kolmogorov cites Prandtl's theory but gives no physical explanation described above.

The concept of a fluid lump in turbulence appears in the book of Townsend as "eddy." In his book, "The Structure of Turbulent Shear Flow" (Townsend, 1956, 1976a), the word "eddy" appears frequently but no clear definition is given. The name of the book has the word "structure," but the concept of the structure function of K41 is not used in the book.

Numerical data of DNS of the turbulent boundary layer can be used to examine the arbitrary two spatial points and two times velocity component in the direction of two points. However, measurements of such a quantity in experiments are almost impossible. On the other hand, the turbulent boundary layer has a directional nature. For example, wall-normal, streamwise, and spanwise directions have different physical characteristics, respectively. The mean and fluctuating velocity data obtained in our measurements with two hot-wires shows the relationship between two spatial points and two times, as discussed in the following.

[DOI: 10.1299/jfst.2024jfst0028]

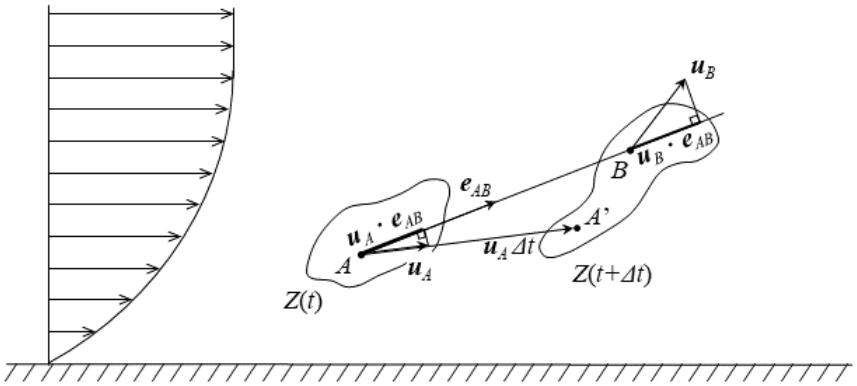

Fig. 3 Schematic of velocity component difference in the case of a flat plate turbulent boundary layer. Where Z is a name that indicates a material lump that includes material point A and moves following the flow field. The point A in Z also moves to A' after Δt.

They have a crucial relationship to the vorticity vector $\boldsymbol{\omega}$, which is defined as,

$$\boldsymbol{\omega} = \left(\frac{\partial u_3}{\partial x_2} - \frac{\partial u_2}{\partial x_3}, \frac{\partial u_1}{\partial x_3} - \frac{\partial u_3}{\partial x_1}, \frac{\partial u_2}{\partial x_1} - \frac{\partial u_1}{\partial x_2}\right). \tag{5}$$

In our experiment, the case of two hot-wires are disposed vertically to the wall, and the distance between them is Δ_2. Since the flat plate turbulent boundary layer is almost two-dimensional, the most important component of $\boldsymbol{\omega}$ in this case is ω_3, and then,

$$\omega_3 = \frac{\partial u_2}{\partial x_1} - \frac{\partial u_1}{\partial x_2} \sim -\frac{\partial u_1}{\partial x_2} \sim -\frac{u_B - u_A}{\Delta_2}, \tag{6}$$

where orthogonal coordinates x_1, x_2, and x_3 indicate the streamwise, wall-normal, and spanwise direction of the boundary layer, respectively. Morton (1984) and Terrington et al. (2022) have conducted related studies that are pertinent to this experiment.

Then, in our experiment, the simultaneous signals of two hot-wires' A and B, separated by wall-normal distance Δ_2, correspond to the x_3-component of vorticity. Similarly, in the case of two-wire distance Δ_3, their output difference corresponds to the x_2-component of $\boldsymbol{\omega}$, as seen in,

$$\omega_2 \sim \frac{\partial u_1}{\partial x_3} \sim \frac{u_B - u_A}{\Delta_3}. \tag{7}$$

Subsequently, the structure function introduced in K41 corresponds to vorticity in the absence of time difference consideration, or it can be associated with circulation along a micro-rectangular path when Stokes' theorem is applied. Since in the turbulent boundary layer, the velocity gradient is very large in the x_2-direction, we must arrange the hot-wire itself parallel to the wall, and considering the structure of the hot-wire probe and the velocity gradient of the flow, the Δ_2 cannot be so small in real experiments, and also, the structure of the probe makes the horizontal distance Δ_3 not so small.

In the research works on the turbulent boundary layer flow from the viewpoint of two spatial points, Favre et al. performed a very large amount of experimental work, and he summarized them in a review paper (Favre, 1965). They consider the wake effect of the upstream probe to the downstream probe, and then probes are distributed on the same streamline. Many years later, Hill (2001) obtained partial differential equations of all order structure functions. These equations were so complicated that he developed computer algebraic software to obtain the many equations. Moreover,

[DOI: 10.1299/jfst.2024jfst0028]

the software is registered on the editorial board of the Journal of Fluid Mechanics for researchers to use. However, Hill did not analyze any concrete real turbulent flow field. After Hill's work, there are studies by Tomkins and Adrian (2003) and Gatti et al. (2020), as mentioned before. In the Annual Review of Fluid Mechanics, two review papers about the coherent structure of turbulence were published (Cantwell, 1981; Robinson, 1991), but note that they did not cite important studies of Favre's. The relationship between Townsend's wall-attached eddies (Cheng et al., 2020) and the present two-point correlations will be considered in the future report. With respect to the correlation between two points in the wall-normal direction, see Baars et al. (2017a, 2017b). However, it appears that no measurements have been made of the structure function of the two-point velocity difference in the wall-normal direction in a turbulent boundary layer, based on the author's search.

In the field of information research, a concept named Kolmogorov's structure function appears. For example, Vereshchagin and Vitányi (2004) describe the nature of data series. The relationship between the informational structure function of the data series and the structure function of turbulence used in the present paper is not evident.

The present authors analyzed the analog hot-wire's digitized data output using Shannon's entropy (Shannon, 1948), Bandt and Pompe's permutation entropy (Bandt and Pompe, 2002) and studied it using Kolmogorov's complexity (Kolmogorov, 1965, 1983). Consult our papers (Ichimiya and Nakamura, 2013, 2017, 2020) for more details.

2. Experimental apparatus, measurement methods, and data processing

2.1 Experimental apparatus and measurement methods

The wind tunnel used was an Eiffel-type one, and in the rectifying section (1920×1920 mm^2) of the wind tunnel, five rectifying wire screens were placed. After the rectifying section, the wind passes through a nozzle with a contraction ratio of 7.5 before reaching the measurement section. The dimensions of the measurement section are 570 mm in height, 620 mm in width, and 2,500 mm in length, and the bottom surface is a Bakelite plate for measurements. A turbulent boundary layer with zero pressure gradient was achieved by adjusting the opposite plate, which is made up of many rectangular plates with long screws. Tripping wires consisting of two cylinders with a diameter of 3 mm are attached 20 mm and 50 mm from the measurement plate's leading edge. The measuring section is shown in Fig. 4. For the measurement section of 2500 mm, the measurement plate and the opposite plate are parallel, and a turbulent boundary layer develops. In the following 500 mm section, the opposite plate linearly approaches the flat plate. Therefore, the flow area converges, then the turbulent boundary layer is accelerated, and the boundary layer relaminarizes. For the turbulent statistics in the relaminarizing process, see Ichimiya et al. (2022). In most downstream sections of 1000 mm, the opposite plate becomes parallel again, and the boundary layer goes to retransition.

The experiment was conducted with a constant unit Reynolds number $U_m / \nu = 2.557 \times 10^5$ m^{-1} (inlet velocity of the measurement section, $U_m \approx 3.8$ m/s). The turbulence intensity in the free stream is 0.6%. The measurements were made at the station where the distance from the flat plate's leading edge is 1600 mm, i.e., 900 mm upstream from the start of the convergence. The boundary layer thickness δ is 36 mm. The Reynolds number is based on the velocity at the boundary layer's outer edge, and the momentum thickness, R_θ is 1047 there. The friction Reynolds number based on the friction velocity and the boundary layer thickness, R_τ is 422 there. Though the effect of the downstream acceleration starts slightly upstream, the pressure gradient is zero, and the relaminarization has not yet begun there. Although this study was conducted at a relatively low Reynolds number, we believe that significant knowledge about the structural function between two points in the wall-normal direction was obtained, which has not been done previously.

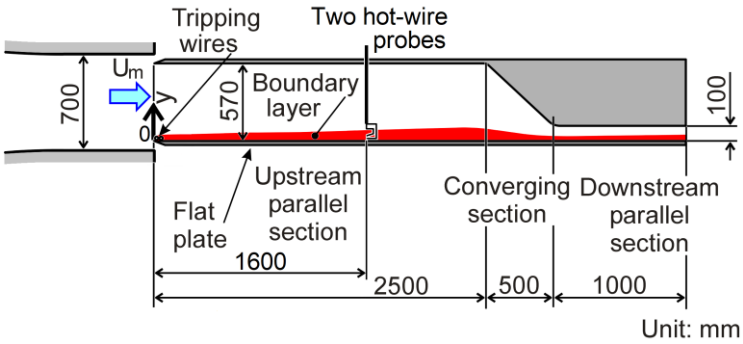

Fig. 4 Schematic of the flow field and coordinate system. The turbulent boundary layer develops in the upstream parallel section. The measurement station is 1600 mm downstream from the leading edge of the flat plate.

[DOI: 10.1299/jfst.2024jfst0028]

The measurement was carried out using two hot-wire probes shown in Fig. 1. Each wire is a single type made of tungsten with a diameter of 5 μm and a length of 1 mm. The ratio of the sensor length and the Kolmogorov length, l/η_K, is approximately 0.5 near the wall. The frequency characteristic of each hot-wire is similar to that of a regular cross-type probe. The calibration of the hot-wire was performed at the same streamwise station but in the free stream. In the calibration, the hot-wire output voltage was linearized to the velocity. The free stream velocity was obtained from the Pitot tube installed at different stations so as not to disturb the flow at the measurement station. The relationship between the free stream velocity and the Pitot tube had been obtained before calibration. In the linearization process, the tangential and binormal velocity components to the sensing element were ignored as small. The two wires are separated in the wall-normal direction. The probe closer to the wall and the one farther from the wall are called the probe-A and the probe-B, respectively. The separation (distance between the two wires), r_y, was adjusted by a caliper (Fig. 1(a)). After the adjustment, the caliper was wrapped in a streamlined cover (Fig. 1(b)). The blockage ratio of the probe support cover is 0.8%. It was confirmed by flow visualization that the cover did not affect the sensing element. The wall-normal position of the probe itself is determined by placing a metal piece on the wall, electrically connecting one end of the probe to the metal, and approaching the metal in 0.01 mm increments. When a current flows between the other end of the probe (sensing element) and the metal, the distance between the two is measured with an accuracy of 0.01 mm. The output voltage of each wire was A/D converted. The data time interval was adjusted according to the acceleration of the free stream to compare with the results at downstream accelerating relaminarization locations for future study. At this 1600 mm downstream station from the leading edge, the time interval was 0.31 ms, and the data number was 84,685.

2.2 Data processing

In the experiment, the caliper of the hot-wire probe was adjusted, and then the separation r_y, was fixed before inserting the probe into the measuring section. Nine separations were used: 0.205, 0.505, 1.005, 2.005, 3.005, 5.005, 10.005, 20.005, and 30.005 mm. (Normalized separations with the viscous length, $r_y^+ = 2.5$, 6.1, 12.2, 24.4, 36.6, 60.9, 122, 243, and 365.) The friction velocity was estimated using the Clauser-chart method. Then, the output voltage of both probes was made proportional to the wind velocity. The probes were traversed in the wall-normal direction in 24 to 25 positions (24 to 25 pairs). In other words, in total, approximately 220 locations (220 pairs) were measured. There are no duplicate pairs within these 220 pairs. This is due to the fact that, throughout the nine separations, probe-A's height (y_A) from the wall is constant at 24~25. Consequently, probe-B's height (y_B) varies For the normalization of the heights from the wall, the boundary layer thickness measured by the probe-A in each experiment, δ_A is used.

3. Experimental results and considerations

3.1 Flow fluctuations' aspects

The time trace of the fluctuating velocities themselves, u_A and u_B, and the velocity difference between them are shown at several pairs here.

First, the pairs in which y_A is within the linear sublayer ($y_A^+ \lesssim 5$) are shown. A total of 4 pairs are shown: (a)($y_A^+ = 2.4$, $y_B^+ = 4.9$) (y_B is also within the linear sublayer), (b)(4.9, 41.4) (y_B is within the buffer layer, $5 \lesssim y_B^+ \lesssim 40$), ($c$)(4.9, 127) ($y_B$ is within the log-law region, $40 \lesssim y_B^+$), and (d)(4.9, 370) (y_B is within the velocity defect region, (0.1~0.2) $\delta \lesssim y_B$). The fluctuating velocity themselves, u_A and u_B, and the velocity difference of the instantaneous velocity are shown in Fig. 5 and 6, respectively. In both figures, velocities are normalized by the velocity at the edge of the boundary layer measured by probe-A, U_{eA}. Subtracting the red signals from the black ones in Fig. 5 corresponds to the signals in Fig. 6. The time range drawn is 0.40 seconds. This corresponds to 845 and 43 times the inner and outer time of the boundary layer there, respectively.

In Fig. 5(a) (2.4, 4.9), both probe heights are close, so both signals also match quite well. Moreover, since the velocity fluctuations themselves are mild in the linear sublayer, the velocity difference signal in Fig. 6(a) is also mild. Signals, however, in the buffer layer and the log-law region (b) and (c) fluctuate finely. Finally, in Fig. 5(d), the fluctuation of u_B within the defect region may be fine. However, since its absolute value is small, it does not contribute much to the velocity difference ($u_B - u_A$) in Fig. 6(d), and the difference reflects the mild fluctuation of u_A.

To verify the above conjecture, we drew the power spectrum of the fluctuating velocity u_A. In addition to the ones that have appeared in Fig. 5 and 6, $y_A^+ = 2.4$, 4.9, 42.6(instead of 41.4), 146(instead of 127), and 365(instead of 370), a total of six locations, including 15.8 that will appear later, are shown in Fig. 7. In the legend, the local Reynolds number based on the Taylor microscale, λ(estimated from local mean velocity times Taylor micro timescale) and rms turbulence

[DOI: 10.1299/jfst.2024jfst0028]

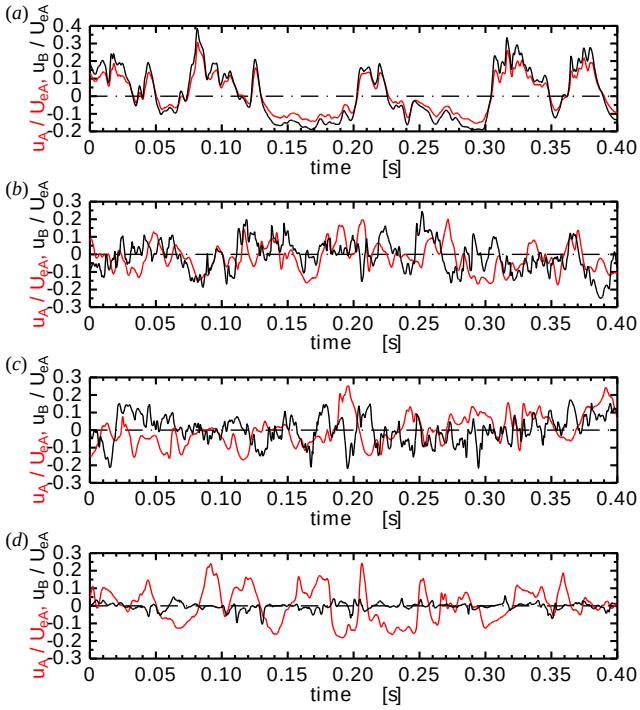

Fig. 5 Time trace of the fluctuating velocity of two points, u_A(red) and u_B(black), where y_A is within the linear sublayer. (*a*)(y_A^+ = 2.4, y_B^+ = 4.9), (*b*)(4.9, 41.4), (*c*)(4.9, 127), (*d*)(4.9, 370).

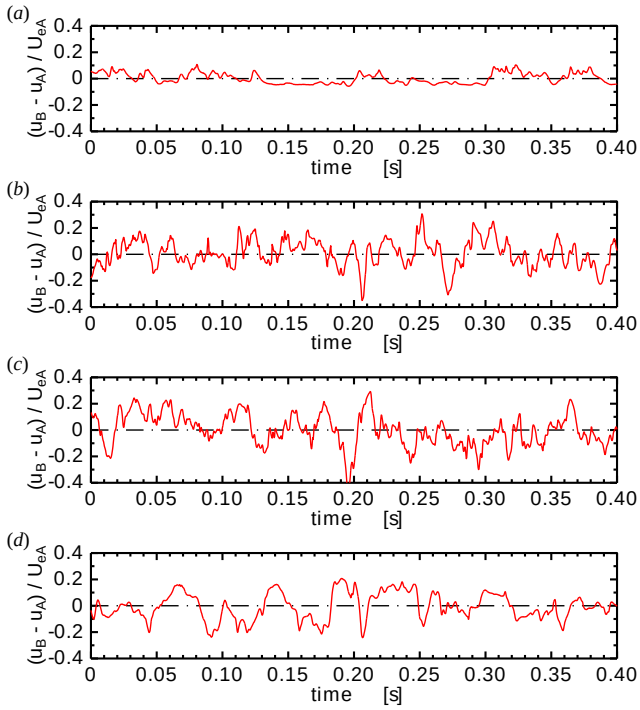

Fig. 6 Time trace of the velocity difference between two points where y_A is within the linear sublayer. Values of y_A^+ and y_B^+ from (*a*) to (*d*) are as Fig. 5.

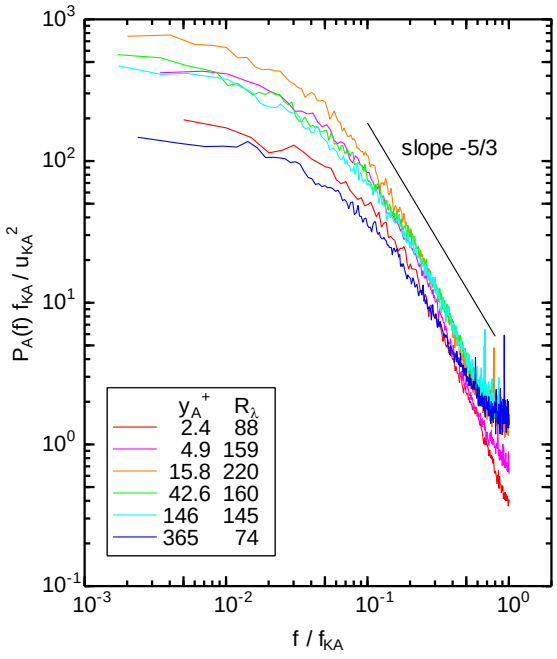

Fig. 7 Power spectrum density function of fluctuating velocity, u_A. Near the wall, the contribution of low frequencies is larger and the contribution of high frequencies is smaller. Away from the wall, the contribution of low frequencies decreases and the contribution of high frequencies increases.

intensity was also written. The frequency range drawn is below the Kolmogorov frequency, f_K.

In the next height, signals of a pair where y_A is within the buffer layer are shown. A total of 3 pairs with y_A^+ = 15.8: (*e*)(y_A^+ = 15.8, y_B^+ = 40.2) (y_B is also within the buffer layer), (*f*)(15.8, 138) (y_B is within the log-law region), and (*g*)(15.8, 381) (y_B is within the velocity defect region) and a total of 2 pairs with y_A^+ = 42.6: (*h*)(42.6, 103) (y_B is within the log-

[DOI: 10.1299/jfst.2024jfst0028]

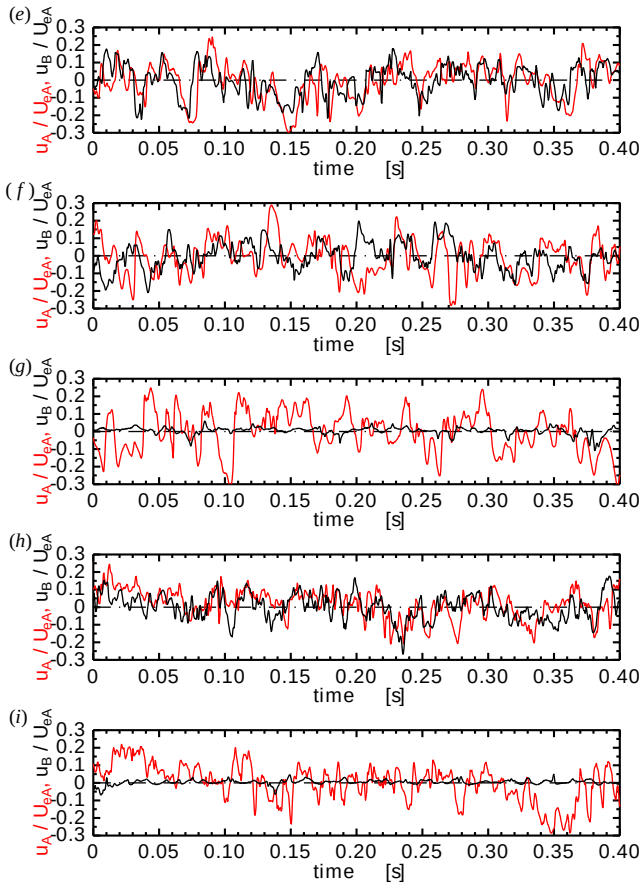

Fig. 8 Time trace of the fluctuating velocity in two points, u_A(red) and u_B(black), where y_A is within the buffer layer. (*e*)(y_A^+ = 15.8, y_B^+ = 40.2), (*f*)(15.8, 138), (*g*)(15.8, 381), (*h*)(42.6, 103), (*i*)(42.6, 408).

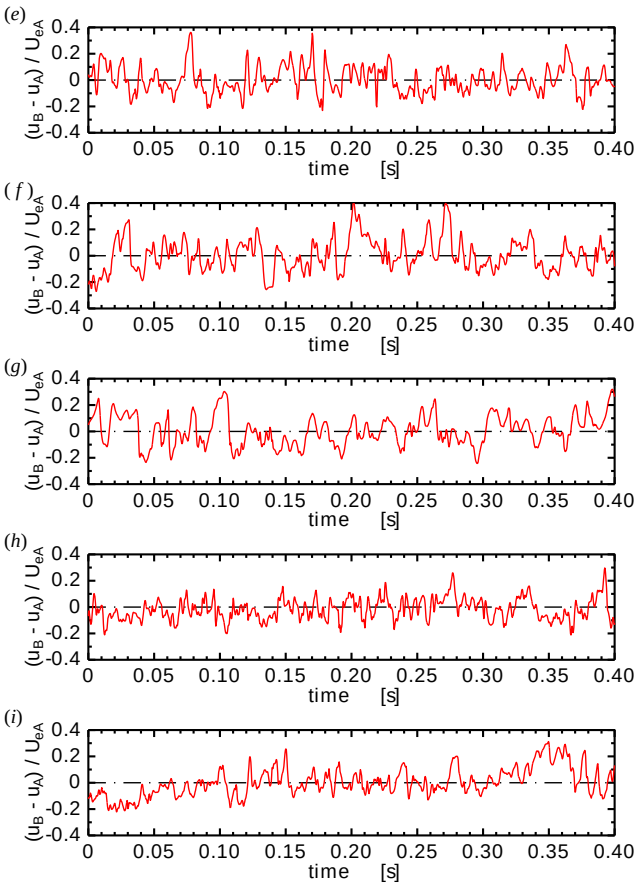

Fig. 9 Time trace of the velocity difference between two points where y_A is within the buffer layer. Values of y_A^+ and y_B^+ from (*e*) to (*i*) are as Fig. 8.

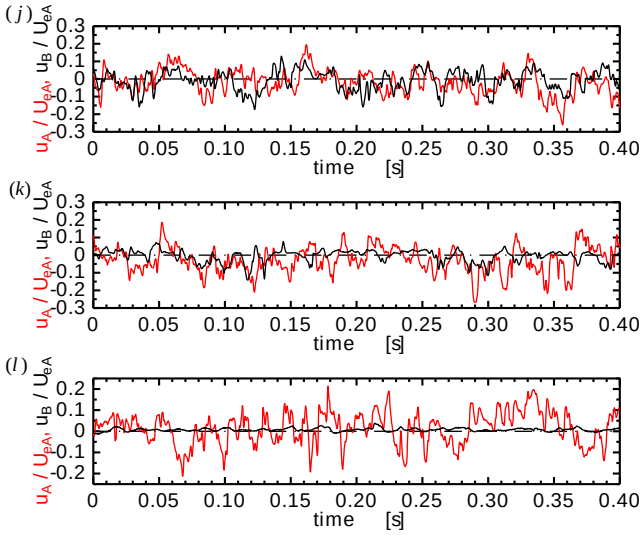

Fig. 10 Time trace of the fluctuating velocity in two points, u_A(red) and u_B(black), where y_A is within the log-law region. (*j*)(y_A^+ = 97.3, y_B^+ = 219), (*k*)(97.3, 341), (*l*)(97.3, 462).

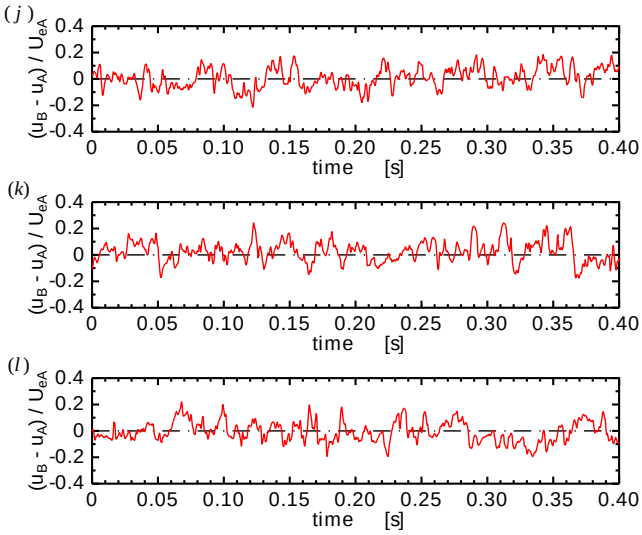

Fig. 11 Time trace of the velocity difference between two points where y_A is within the log-law region. Values of y_A^+ and y_B^+ from (*j*) to (*l*) are as Fig. 10.

law region), and (*i*)(42.6, 408) (y_B is within the defect region) are drawn in Fig. 8 and 9. In (*e*)(15.8, 40.2), since the heights of both probes are also close, both signals in Fig. 8(*e*) overlap well when shifted slightly in time. The events of u_B come slightly earlier than that of u_A. For the quantification of this time difference, a spatiotemporal correlation

[DOI: 10.1299/jfst.2024jfst0028]

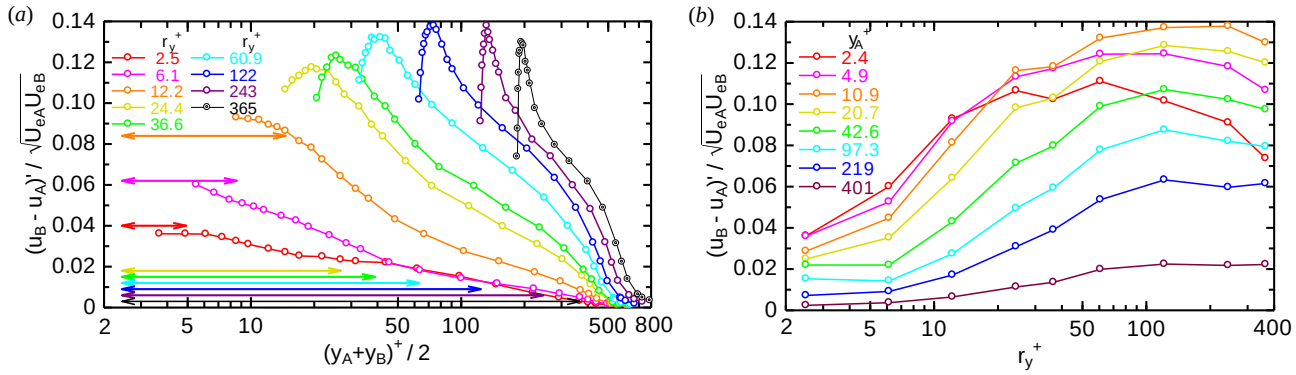

Fig. 12 Fluctuating velocity difference between two points as a function of (*a*) wall-normal distance and (*b*) two-point separation. Horizontal arrows with respective colors in (*a*) represent the range between probe-A and B when probe-A is the nearest height from the wall, $y_A^+ = 2.4$. In (*a*), tracing a certain colored distribution in the right direction in the figure means the heights of both probes increase simultaneously while keeping the separation between them fixed. In (*b*), tracing a specific colored distribution in the right direction in the figure entails moving probe-B away from the wall while keeping probe-A stationary.

coefficient between the two signals is useful. We estimated it previously (Ichimiya et al., 2022) and showed that the coherent structure in the turbulent boundary layer tilts downstream as it moves away from the wall.

Finally, signals of a pair where y_A is within the log-law region are shown. A total of 3 pairs: (*j*)($y_A^+ = 97.3$, $y_B^+ = 219$) (y_B is also within the log-law region or defect region), (*k*)(97.3, 341) (y_B is within the defect region), and (*l*)(97.3, 462) (y_B is within the defect region) are drawn in Fig. 10 and 11. When both heights are not so far (*j*) (97.3, 219), both signals in Fig. 10(*j*) are also close in time, i.e., the deviation in the horizontal direction is small. On the other hand, since a difference between the same time is recognizable, the velocity difference is not zero in Fig. 11(*j*).

To show the magnitude of the fluctuating velocity difference shown above quantitatively, the distribution of its root mean square (rms) value, $(u_B - u_A)'$ is shown in Fig. 12. Where the prime means rms value. The values are normalized by the velocity at the boundary layer's edge, measured by each probe.

Figure. 12(*a*) shows the separation between two probes as a parameter. Values are shown at the midpoint of both probes. Tracing a certain colored distribution in the right direction in the figure means the heights of both probes increase simultaneously while keeping the separation between them fixed. In addition, as a guide for the separation, the two points closest to the wall ($y_A^+ = 2.4$, $y_B^+ = 2.4 + r_y^+$) are connected with an arrow of the same color. That is, the mathematical midpoint at both ends of the arrow (which is different from the midpoint on the diagram because of a logarithmic display) corresponds to the leftmost point of each distribution.

When the separation is small ($r_y^+ \leqq 12.2$), the rms value decreases monotonically with the distance from the wall. The reason for this is that since the separation is small, the "phases" of both fluctuation match, as shown in Fig. 5(*a*) and 6(*a*), so the velocity difference becomes smaller. In this condition, when both probes move away from the wall while maintaining phase matching, the fluctuating velocity initially drops.

On the other hand, when the separation increases and becomes more than 24.4 (yellow), the fluctuating velocity difference increases at first, reaches a maximum, and then decreases. The reason why it increases at first is that, as inferred above, in this condition, y_B is large, so its fluctuating velocity is small, and as Fig. 5(*d*), the difference $(u_B - u_A)$ is approaching $(0 - u_A) = -u_A$. When both probes move away from the wall in this condition, y_A approaches the maximum position of the fluctuating velocity distribution ($y^+ = 10 \sim 15$) (see, e.g., Spalart, 1988, Fig. 13), so the difference $(u_B - u_A)$ increases. In fact, the y_A^+ position of the maximum values in Fig. 12(*a*) ($r_y^+ = 243$ (purple), $(y_A + y_B)^+/2 = 133$) is = 10.9. Which is close to the maximum position ($y^+ = 10 \sim 15$). When y_A exceeds the maximum position, the velocity difference decreases.

Figure 12(*b*) shows the probe separation changes in the fluctuating velocity difference with the height of probe-A as a parameter. In this type, tracing a certain colored distribution in the right direction in the figure means moving the probe-B away from the wall while keeping the probe-A fixed. Eight values of y_A were used as examples.

For any parameter y_A, as the separation increases, the fluctuating velocity difference increases, then peaks, and finally decreases. The reason for this is that when the separation is small, the fluctuation "phases" between both fluctuating velocities match as described above, so the fluctuating velocity difference becomes small. On the other hand, as the

[DOI: 10.1299/jfst.2024jfst0028]

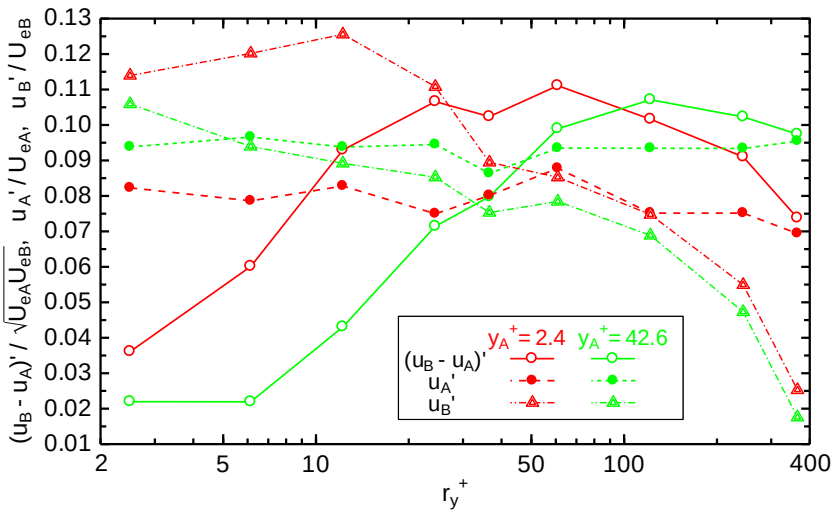

Fig. 13 Fluctuating velocity difference between two points, $(u_B-u_A)'$, and fluctuating velocity at a point, u_A' and u_B'. $y_A^+ =$ 2.4(red), 42.6(green). Open circle; $(u_B-u_A)'$, closed circle; u_A', triangle; u_B'. At first, $(u_B-u_A)'$ is smaller than u_A' alone. As r_y increases $(u_B-u_A)'$ increases and exceeds u_A'. Further, as r_y increases, $(u_B-u_A)'$ decreases because of the decrease of u_B.

separation increases, the "phases" do not match as shown in Fig. 5(b), 5(c), 6(b), and 6(c). So, the fluctuating velocity difference increases. When these out-of-phase units, u_A and u_B, are combined, they attain their maximum value. As the separation increases further, the amplitude of u_B becomes smaller, as described above, and (u_B-u_A) approaches $-u_A$, so it decreases. Then, since the velocity difference in the rightmost point of each parameter is closest to the single u_A', the parameter y_A^+ for which the rightmost point is maximum among the eight rightmost points, $y_A^+ = 10.9$ (orange) is the maximum position of the fluctuating velocity distribution ($y^+ = 10$ to 15).

As discussed above, when y_B is extremely far from the wall, as shown in Fig. 5(d), it is expected that the velocity difference (u_B-u_A) will be close to the single value $-u_A$. We will verify it here. Take $y_A^+ = 2.4$ (red) and 42.6 (green) as examples, which are shown in Fig. 13.

For both y_A, at first (when y_B is small), $(u_B-u_A)'$ is smaller than u_A' alone. In other words, it is validated that the "phases" of fluctuations of u_A and u_B almost match and cancel each other out. As r_y, i.e., y_B increases, however, $(u_B-u_A)'$ increases, demonstrating that u_A and u_B are out of phase. As r_y further increases, $(u_B-u_A)'$ exceeds u_A' in $r_y^+ > 10$ and 48 at $y_A^+ = 2.4$ and 42.6, respectively. This is because both positions are far enough away that there is no correlation between them. Therefore, the long-time average of (u_B-u_A) is almost the same as that of (u_B+u_A), so it is larger than u_A' alone. This is further demonstrated by estimating the change in the spatial correlation coefficient between u_A and u_B as a function of the separation. This will be clarified in a later section.

Further, as r_y increases, $r_y^+ \gtrsim 61$ and 122 at $y_A^+ = 2.4$ and 42.6, respectively, $(u_B-u_A)'$ decreases because of the decrease of u_B, it becomes approximately equal to u_A'. The decrease of u_B can be confirmed by the rms distribution (triangle symbols).

The distribution of the probability density function (pdf) of the fluctuation velocity difference (u_B-u_A) is shown in Fig. 14 for 12 pairs: The pairs are the same as Fig. 6(a)~(d), Fig. 9(e)~(i), and Fig. 11(j)~(l). The abscissa and ordinate are made dimensionless by the rms value. The range of the abscissa is divided by 100 between the maximum and minimum values. Values of the skewness and flatness factors of the fluctuating velocity difference, $\overline{(u_B-u_A)^3}/(u_B-u_A)'^3$ and $\overline{(u_B-u_A)^4}/(u_B-u_A)'^4$, respectively, are also shown in the legend. The distribution area in any figure equals unity since the same quantity renders both axes dimensionless

In the fluctuating velocity difference signals (Fig. 6, 9, and 11), in cases (b) and (c) where the distribution shape and absolute values on the positive and negative sides are almost the same, the pdfs in Fig. 14 are also almost symmetrical between the positive and negative sides and the skewness factor is small. In cases (a), (e), (f), (g), (h), and (i), where the appearance time is short, but the absolute value is large on the positive velocity side, the pdf tails on the positive velocity side are long, and the skewness factors are positive. On the other hand, in case (d), where the appearance time is short, but the absolute value is large on the negative velocity side, the tail on the negative velocity side is long, and the skewness

[DOI: 10.1299/jfst.2024jfst0028]

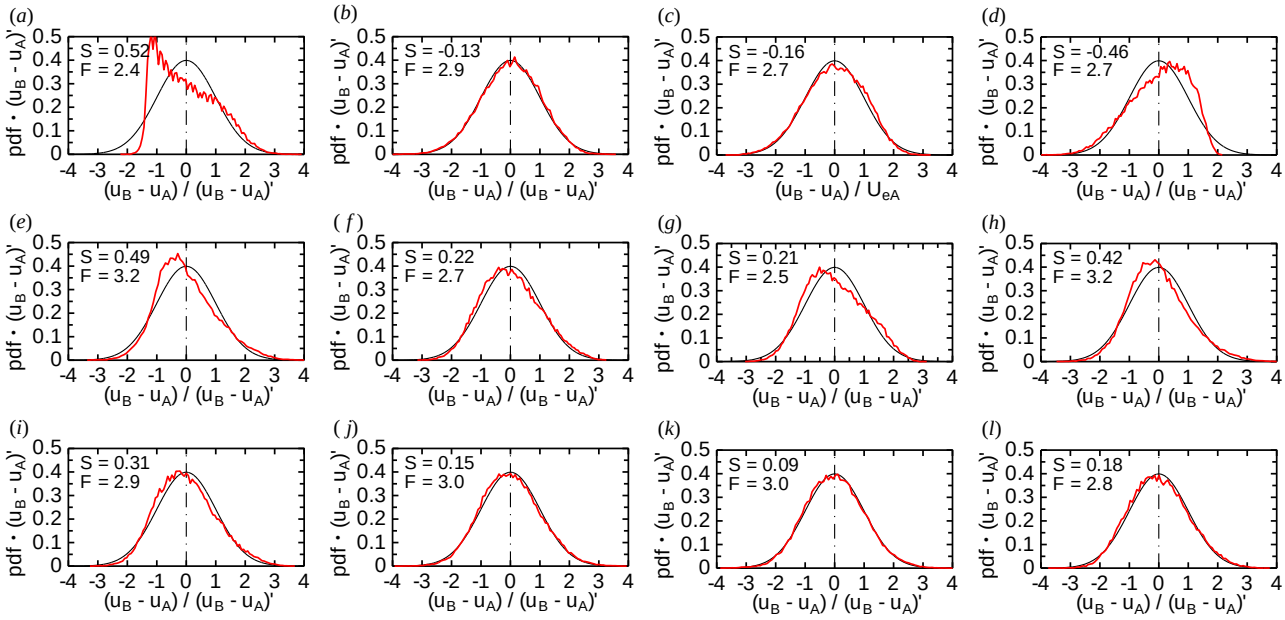

Fig. 14 The probability density function of fluctuating velocity difference(red) and Gaussian distribution(black). The values of y_A^+ and y_B^+ are shown in Fig. 6 for (*a*) to (*d*), Fig. 9 for (*e*) to (*i*), and Fig. 11 for (*j*) to (*l*).

factor is negative. In cases (*j*), (*k*), and (*l*), where the probes are in the logarithmic region, or the defect region, the difference between similar fluctuating velocities causes the distribution shape to be symmetrical and close to the Gaussian distribution. Therefore, the skewness factor is small, and the flatness factor is close to 3.

3.2 Fluctuating vorticity and structure function

The difference in the streamwise instantaneous velocity, $\tilde{u}$, at the same time between two close points separated in the y direction, $-\Delta\tilde{u}/\Delta y$, is approximated to the instantaneous vorticity, $\tilde{\omega}_z$ as Eq. (5). This fluctuation is obtained in this section. First, the expressions for instantaneous, time-averaged, and fluctuating vorticities are listed below.

$$\tilde{\omega}_z = \frac{\partial\tilde{v}}{\partial x} - \frac{\partial\tilde{u}}{\partial y} \sim -\frac{\partial\tilde{u}}{\partial y} \sim -\frac{\Delta\tilde{u}}{\Delta y} = -\frac{\tilde{u}_B-\tilde{u}_A}{y_B-y_A} = -\frac{(U_B+u_B)-(U_A+u_A)}{y_B-y_A}\ , \tag{8}$$

$$\therefore \Omega_z = \overline{\tilde{\omega}_z} \sim -\frac{\overline{(U_B+u_B)-(U_A+u_A)}}{y_B-y_A} = -\frac{U_B-U_A}{y_B-y_A}\ , \tag{9}$$

$$\therefore \omega_z = \tilde{\omega}_z - \Omega_z \sim -\frac{u_B-u_A}{y_B-y_A}\ , \tag{10}$$

$$\therefore \omega_z' = \sqrt{\overline{\omega_z^2}} \sim \frac{\sqrt{\overline{(u_B-u_A)^2}}}{y_B-y_A} = \frac{(u_B-u_A)'}{r_y} = \frac{\sqrt{B(y_A,r_y)}}{r_y}\ . \tag{11}$$

Where both overbar and capital letters mean time-averaged quantities and lowercase letters mean fluctuating quantities. In this way, the structure function $B(y_A,r_y) = \overline{[u(y_A+r_y)-u(y_A)]^2} = \overline{(u_B-u_A)^2}$, and the rms value of the fluctuating vorticity are related to each other.

Figure 15 shows the fluctuating vorticity's rms value, ω_z', made dimensionless by the velocity at the boundary layer's edge measured with each probe and the boundary layer thickness measured with probe-A,

$$\frac{\omega_z'\delta_A}{\sqrt{U_{eA}U_{eB}}} \sim \frac{(u_B-u_A)'/\sqrt{U_{eA}U_{eB}}}{r_y/\delta_A}. \tag{12}$$

[DOI: 10.1299/jfst.2024jfst0028]

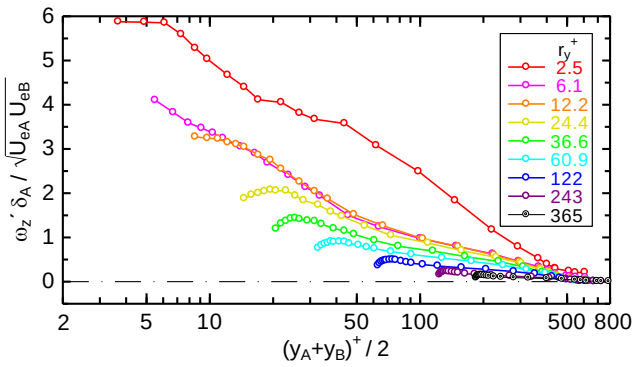

Fig. 15 Fluctuating vorticity as a function of wall-normal distance. The vorticity decreases monotonically with the distance from the wall.

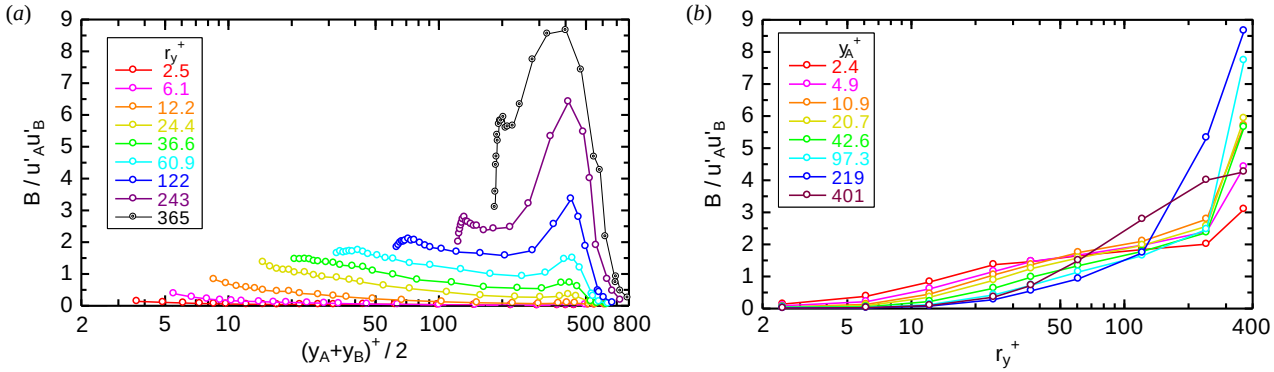

Fig. 16 Structure function as a function of (*a*) wall-normal distance and (*b*) two-point separation. Away from the wall, the structure function becomes large.

In Fig. 15, if the value of the parameter r_y^+ is increased while the position on the abscissa is fixed, this is equivalent to moving probe-A closer to the wall and moving probe-B away from the wall while keeping the center position between the two probes fixed. At this point, the vorticity diminishes, reflecting a decrease in accuracy as the separation increases. For the minimum separation, $r_y^+ = 2.5$, the vorticity decreases monotonically with the distance from the wall. This trend is reasonable because it is qualitatively the same as the fluctuating velocity distribution.

Figure 16 shows the distribution of the structure function, $B(y_A, r_y) = \overline{[u(y_A+r_y) - u(y_A)]^2} = \overline{(u_B - u_A)^2}$. They are shown in two ways, as Fig. 12(*a*) and (*b*). Figure 12 shows the distributions equivalent to the square of the structure function made dimensionless by the boundary layer edge velocity. On the other hand, in Fig. 16, the structure function itself is made dimensionless by the rms value of the local fluctuating velocity of both probes. Since the fluctuating velocity is a representative value of the turbulence intensity, this style can be considered as a relative value that the physical value of the structure function has with respect to the representative value of the turbulence intensity. Away from the wall, since the denominator, i.e., the fluctuating velocity decreases, the structure function becomes large.

3.3 Spatial correlation coefficient

From the velocity measurements at two spatial points, we can find a spatial correlation. Here, a simultaneous two-point spatial correlation coefficient is shown.

Figure 17(*a*) shows the separation between two points as a parameter. The correlation coefficient increases with the distance from the wall. This means that as one moves away from the wall while keeping the separation constant, the length over which the correlation is maintained increases. That is, the large eddy prevails, and *vice versa*. Only with the non-dimensional separation of 2.5 (red), however, the correlation is always about 0.99.

Figure 17(*b*) shows the probe separation changes. The correlation coefficient has a typical distribution shape, decreasing from unity as the separation increases. With large y_A, as the separation increases, i.e., y_B moves away from y_A, the decrease from unity becomes slower. This means that as moving away from the wall, the large eddy prevails as above. In Fig. 17(*a*), when the separation is large, the correlation reaches a minimum at $(y_A + y_B)^+/2 \approx 400$. This corresponds

[DOI: 10.1299/jfst.2024jfst0028]

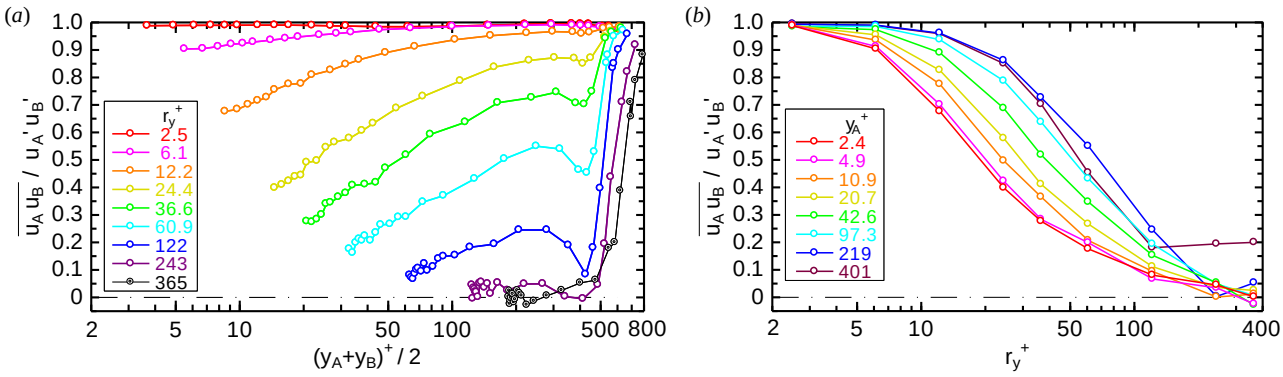

Fig. 17 Spatial correlation coefficient as a function of (a) wall-normal distance and (b) two-point separation. The correlation coefficient increases with the distance from the wall and decreases with the two-point separation.

to a situation in Fig. 17(*b*). For example, in the region of $30 \lesssim r_y^+ \lesssim 150$, the distribution with $y_A^+ = 401$ (purple) is smaller than that with $y_A^+ = 219$ (blue). In this situation, probe-A is located within the boundary layer, and probe-B is located within the free stream. As a result, the correlation between the two positions is reduced.

In §3.1, the fluctuating velocity difference $(u_B - u_A)'$ became larger than u_A' alone while moving away from the wall (Fig. 13). It was assumed that since both points were so far, the correlation became small. This assumption is verified now. At the inverted positions, i.e., $r_y^+ = 10$ and 48 at $y_A^+ = 2.4$ and 42.6, respectively, in Fig. 17(*b*), the correlation coefficients are indeed 0.8 and 0.4, respectively, demonstrating that the correlation is getting worse.

4. Discussions

In the following, we will discuss the nature of turbulence research. Every turbulence researcher, irrespective of the theoretical, experimental, and computational field, knows that the physical insight into turbulence has a central importance in understanding the turbulent flow field since the randomness of its space-time compels us to summarize the structure. Without that notion, we meet intractable information of the sensor's output or computed array numbers from a computer that solves Navier-Stokes equations directly.

Historically, Prandtl's intuition introduced the mixing length assumption, which means a lump of fluid moves, holding its momentum perpendicular to the main flow (Prandtl, 1925). In the classical book of turbulence, Hinze (1975b) proposed his conceptual physical model of wall turbulence. Davidson (2015b) shows many cartoons of turbulent flow to aid the readers of his book in obtaining the physics of turbulent fields.

Recently, Townsend's attached eddy model presented in his book (Townsend, 1976b) has been extensively discussed in a review paper (Marusic and Monty, 2019), in which Townsend's conical eddy attached to the wall is drawn. These various concepts proposed by many authors help our insight into turbulence, but they are qualitative in nature. The results obtained by the use of two hot-wire probes in the present paper are essentially dynamic and quantitative measures of turbulence. This research character helps us to obtain a deep understanding of turbulence.

5. Conclusions

The streamwise velocity between two points separated in the wall-normal direction in a turbulent boundary layer under zero pressure gradient was measured, and signals of the fluctuating velocity difference at the same time, probability density function, fluctuating vorticity, structure function, and spatial correlation coefficient were obtained. The following conclusions were obtained.

(1) When the spatial separation between two points is small, the fluctuating velocity difference decreases monotonically as the two points move away from the wall. On the other hand, as the spatial separation increases, the similarity between the two fluctuating velocities decreases. In addition, the fluctuating velocity at the nearer point from the wall becomes dominant. When moving away from the wall, the fluctuating velocity difference first increases, then reaches a maximum, and finally decreases.

[DOI: 10.1299/jfst.2024jfst0028]

(2) When both positions are within the logarithmic region or defect region, the velocity difference is made between similar fluctuating velocities. Hence, the probability density function distribution shape is symmetrical with respect to positive and negative values, close to the Gaussian distribution.

(3) The fluctuating vorticity decreases monotonically as it moves away from the wall, regardless of the spatial separation.

(4) The structure function increases as the separation increases.

(5) Away from the wall, the length over which the correlation is maintained increases, resulting in a large eddy.

Acknowledgement

The authors would like to thank Mr. M. Nakata for helping with the experiments and Ms. M. Jige for helping with the drawings. The authors acknowledge the reviewers for their comments, which greatly improved this paper.

References

Anselmet, F., Gagne, Y., Hopfinger, E. J. and Antonia, R. A., High-order velocity structure functions in turbulent shear flows, Journal of Fluid Mechanics, Vol. 140 (1984), pp.63–89.

Baars, W. J., Hutchins, N. and Marusic, I., Reynolds number trend of hierarchies and scale interactions in turbulent boundary layers, Philosophical Transactions of the Royal Society A, Vol. 375, Issue 2089(2017a), DOI:10.1098/rsta.2016.0077.

Baars, W. J., Hutchins, N. and Marusic, I., Self-similarity of wall-attached turbulence in boundary layers, Journal of Fluid Mechanics, Vol. 823(2017b), DOI:10.1017/jfm.2017.357.

Bandt, C. and Pompe, B., Permutation entropy: A natural complexity measure for time series, Physical Review Letters, Vol. 88, No. 17 (2002), DOI:10.1103/PhysRevLett.88.174102.

Cantwell, B. J., Organized motion in turbulent flow, Annual Review of Fluid Mechanics, Vol. 13 (1981), pp.457–515.

Cheng, C., Li, W., Lozano-Durán, A. and Liu, H., Uncovering Townsend's wall-attached eddies in low-Reynolds-number wall turbulence, Journal of Fluid Mechanics, Vol. 889 (2020), DOI:10.1017/jfm.2020.100.

Davidson, P. A., Turbulence, 2nd ed. (2015a), pp.88–97, Oxford University Press.

Davidson, P. A., Turbulence, 2nd ed. (2015b), pp.135–136, Oxford University Press.

Favre, A. J., Review on Space-Time Correlations in Turbulent Fluids, Journal of Applied Mechanics, Vol. 32, No. 2 (1965), pp.241–257.

Garratt, J. R., The Atmospheric Boundary Layer (1992), Cambridge University Press.

Gatti, D., Chiarini, A., Cimarelli, A. and Quadrio, M., Structure function tensor equations in inhomogeneous turbulence, Journal of Fluid Mechanics, Vol. 898 (2020), DOI:10.1017/jfm.2020.399.

Goit, J. P. and Meyers, J., Analysis of turbulent flow properties and energy fluxes in optimally controlled wind-farm boundary layers, Journal of Physics: Conference Series, Vol. 524 (2014), DOI:10.1088/1742-6596/524/1/012178.

Hill, R., Equations relating structure functions of all orders, Journal of Fluid Mechanics, Vol. 434 (2001), pp.379–388.

Hinze, J. O., Turbulence, 2nd ed. (1975a), pp.30–44, McGraw-Hill.

Hinze, J. O., Turbulence, 2nd ed. (1975b), p.683, McGraw-Hill.

Ichimiya, M. and Nakamura, I., Randomness representation in turbulent flows with Kolmogorov complexity (In mixing layer), Journal of Fluid Science and Technology, Vol. 8, No. 3 (2013), pp.407–422.

Ichimiya, M. and Nakamura, I., Analysis of laminar-turbulent transition process in mixing layer with various information measures, Transactions of the JSME (in Japanese), Vol. 83, No. 845 (2017), DOI:10.1299/transjsme.16-00497.

Ichimiya, M. and Nakamura, I., Various information and complexity measures for analyzing the laminar-turbulent transition process in mixing layer (Analysis of fluctuating vorticity and turbulent energy dissipation rate), Transactions of the JSME (in Japanese), Vol. 86, No. 890 (2020), DOI:10.1299/transjsme.20-00130.

Ichimiya, M., Nakamura, I. and Nakata, M., Relaminarization of accelerated turbulent boundary layer under favorable pressure gradient with sink flow type (Coherent structure and two-point statistics), Transactions of the JSME (in Japanese), Vol. 88, No. 909 (2022), DOI:10.1299/transjsme.22-00010.

Japanese Society of Steel Construction ed., Structure Endure Engineering to Wind (1997), pp.394–407, Tokyo Denki University Press (in Japanese).

[DOI: 10.1299/jfst.2024jfst0028]

Kármán, T. and Howarth, L., On the statistical theory of isotropic turbulence, Proceedings of the Royal Society of London, A, Vol. 164, Issue 917 (1938), pp.192–215.

Kolmogorov, A. N. (English translation by Levin, V.), The local structure of turbulence in incompressible viscous fluid for very large Reynolds numbers, Proceedings of the Royal Society of London, A, Vol. 434, Issue 1890 (1991), pp.9–13. (Original; Dokl. Acad. Nauk SSSR 30–4(1941), pp.301–305 (in Russian).)

Kolmogorov, A. N., Three approaches to the quantitative definition of information, Problems of Information Transmission, Vol. 1, No. 1 (1965), pp.1–7.

Kolmogorov, A. N., Combinatorial foundations of information theory and the calculus of probabilities, Russian Mathematical Surveys, Vol. 38, No. 4 (1983), pp. 29–40.

Marusic, I. and Monty, J. P., Attached eddy model of wall turbulence, Annual Review of Fluid Mechanics, Vol. 51 (2019), pp.49–74.

Morton, B. R., The generation and decay of vorticity, Geophysical and Astrophysical Fluid Dynamics, Vol. 28, Issue 3-4 (1984), pp.277–308.

Pope, S. B., Turbulent Flows (2000), pp. 189–206, Cambridge University Press.

Prandtl, L., Bericht über Untersuchungen zur ausgebildeten Turbulenz, Zeitschrift für Angewandte Mathematik und Mechanik (Journal of Applied Mathematics and Mechanics), Vol. 5, Issue 2 (1925), pp.136–139 (in German).

Robinson, S. K., Coherent motions in the turbulent boundary layer, Annual Review of Fluid Mechanics, Vol. 23 (1991), pp.601–639.

Schlichting, H. and Gersten, K., Boundary-Layer Theory, 8th Revised and Enlarged ed. (2000), pp.18–24, Springer.

Shannon, C. E., A mathematical theory of communication, The Bell System Technical Journal, Vol. 27 (1948), pp.379–423, 623–656.

Spalart, P. R., Direct simulation of a turbulent boundary layer up to $R_\theta = 1410$, Journal of Fluid Mechanics, Vol. 187 (1988), pp.61–98.

Taylor, G. I., Statistical theory of turbulence, Parts 1-4, Proceedings of the Royal Society of London, A, Vol. 151, Issue 873 (1935), pp.421–478.

Terrington. S. J., Hourigan, K. and Thompson, M. C., Vorticity generation and conservation on generalised interfaces in three-dimensional flows, Journal of Fluid Mechanics, Vol. 936 (2022), DOI:10.1017/jfm.2022.91.

Tomkins, C. D. and Adrian, R. J., Spanwise structure and scale growth in turbulent boundary layers, Journal of Fluid Mechanics, Vol. 490 (2003), pp.37–74.

Townsend, A. A., The Structure of Turbulent Shear Flow (1956), pp.107,120–130, Cambridge University Press.

Townsend, A. A., The Structure of Turbulent Shear Flow, 2nd ed. (1976a), pp.54,62–64,118–119,122–124, Cambridge University Press.

Townsend, A. A., The Structure of Turbulent Shear Flow, 2nd ed. (1976b), pp.152–153, Cambridge University Press.

Vereshchagin, N. K. and Vitányi, P. M. B., Kolmogorov's structure functions and model selection, IEEE Transactions on Information Theory, Vol. 50, No. 12 (2004), pp.3265–3290.

Wyngaard, J. C., Turbulence in the Atmosphere (2010), Cambridge University Press.

[DOI: 10.1299/jfst.2024jfst0028]